BIOCHEMISTRY
including biophysical chemistry & molecular biology

Article

pubs.acs.org/biochemistry

Competition between Tryptophan Fluorescence and Electron Transfer during Unfolding of the Villin Headpiece

William W. Parson*

Department of Biochemistry, University of Washington, Seattle, Washington 98195-7350, United States

Supporting Information

ABSTRACT: The 35-residue, C-terminal headpiece subdomain of the protein villin folds to a stable structure on a microsecond time scale and has served as a model system in numerous studies of protein folding. To obtain a convenient spectroscopic probe of the folding dynamics, Kubelka et al. introduced an ionized histidine residue at position 27, with the expectation that it would quench the fluorescence of tryptophan 23 in the folded protein by extracting an electron from the excited indole ring [Kubelka, J., et al. (2003) *J. Mol. Biol. 329*, 625−630]. Although the fluorescence yield decreased as anticipated when the protein folded, it was not clear that the side chains of the two residues were sufficiently close together for electron transfer to compete effectively with fluorescence. Here, hybrid classical−quantum mechanical molecular dynamics simulations are used to examine the rates of transfer of an electron from the excited tryptophan to various possible acceptors in the modified headpiece and a smaller fragment comprised of residues 21−27 (HP7). The dominant reaction is found to be transfer to the amide group on the carboxyl side of W23 (amide *a*24). This process is energetically favorable and has a large coupling factor in the folded protein at 280 K but becomes unfavorable as HP7 unfolds at higher temperatures. Changes in electrostatic interactions of the solvent and other parts of the protein with the indole ring and *a*24 contribute importantly to this change in energy.

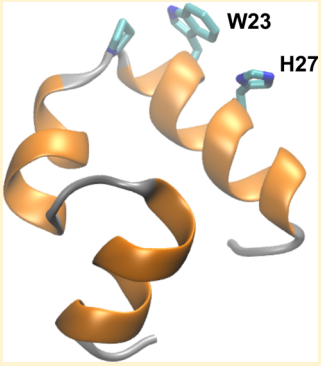

The 35-residue C-terminal subdomain of the villin headpiece is one of the smallest proteins that fold autonomously to a stable structure.[2,3] Its exceptionally rapid folding has stimulated numerous studies by both experimental[1,4−20] and theoretical[21−39] approaches. Measurements of tryptophan fluorescence have figured prominently in these studies. The headpiece contains a single tryptophan residue (W23), which is located in the N-terminal α-helix [α3 (Figure 1)]. To increase the sensitivity of the fluorescence to folding of the protein, Kubelka et al.[1,8] substituted histidine for asparagine N27, four residues away in the same helix. Studies of other systems have shown that the imidazolium ring of a protonated histidine residue often can quench tryptophan fluorescence by extracting an electron from the excited indole ring, provided that the two rings are sufficiently close together.[40−45] As expected, the fluorescence of the modified protein (HP35) was quenched strongly relative to the fluorescence of the peptide fragment acetyl-WKQQH but approached that of the peptide when the temperature was increased above ∼350 K or a denaturant was added.[1,8,20] This quenching was not seen in the peptide that had asparagine at position 27.[46] Temperature-jump experiments revealed further that the fluorescence quantum yield (Φ_f) in the peptide containing protonated histidine 27 increased in two steps with time constants of approximately 70 ns and 4 μs. The slower step also was seen by measuring changes in infrared absorption[19] or quenching of the tryptophan's excited triplet state by a cysteine residue placed at the N-terminus.[5,16]

The structural basis of the fluorescence changes seen in the temperature-jump experiments has been puzzling. Molecular dynamics (MD) simulations suggest that the distance between the ring systems of W23 and H27 approaches its final distribution in concert with formation of the first turn of

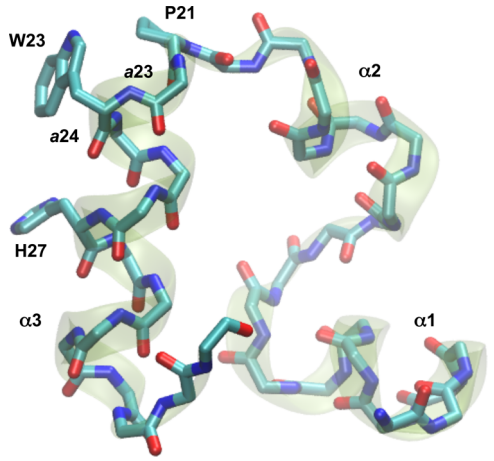

Figure 1. Structure of the villin headpiece with N27 replaced with histidine (HP35).[17] The protein backbone, the side chains of W23 and H27, and the P21 ring are shown in licorice representations colored by atom type, with a cartoon of the secondary structure superimposed. Amide groups *a*23 and *a*24 and helices α1−α3 are labeled.

Received: April 17, 2014
Revised: June 23, 2014
Published: June 27, 2014

   dx.doi.org/10.1021/bi5004712 | *Biochemistry* 2014, 53, 4503−4509

helix α3, preceding adoption of a stable tertiary structure.[21,25,30] Tusell and Callis[29] noted, however, that the mean distance between the two rings appears to be too large for facile electron transfer.[29] They therefore suggested that fluorescence quenching depends on rare excursions to conformations that bring the rings closer together, and that the propensity to visit these conformers changes as HP35 folds. However, the protein was found in such "close" conformers only ~4% of the time, and the frequency of their occurrence was similar in MD simulations at 280 and 400 K. The authors estimated that a population of 40% would be needed to account quantitatively for the quenching. In addition, the fluorescence quenching was less sensitive to pH than would be expected if it required H27 to be protonated.[46]

This work examines the mechanism of tryptophan fluorescence quenching during MD simulations of HP35 and a peptide subfragment, *N*-acetyl-PLWKQQH-NH_2 [HP7 (Figure 2)], using a treatment of electron-transfer dynamics that was developed recently by McMillan et al.[44] Unexpectedly, the dominant quenching mechanism appears to be the transfer of an electron to a backbone amide group, rather than to the imidazolium ring of H27. The radical pair generated by the transfer of an electron to the amide is stabilized by electrostatic interactions that become less favorable as HP7 unfolds.

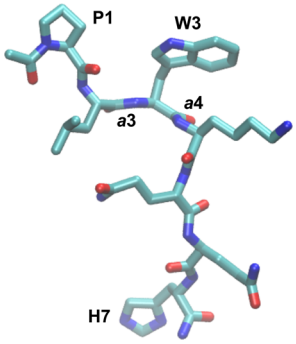

Figure 2. Representative snapshot of the unfolded HP7 peptide after 8 ns at 380 K. The non-hydrogen atoms are shown in licorice representations colored by atom type. Residues P1, W3, and H7 and amide groups *a*3 and *a*4 are labeled.

METHODS

Models of HP35 for MD simulations were generated by adding hydrogens to the crystal structure (Protein Data Bank entry 1YRF),[17] protonating the side chain of H27, and embedding the protein in approximately 1100 water molecules constrained to a sphere with a radius of 20 Å. Random placements of the water were used to obtain different initial systems. After energy minimization by MD for 10 ps at 30 K, trajectories were continued in the ground electronic state for 4 ns at 280 K. For some calculations, H27 was replaced with asparagine. Models of the seven-residue fragment acetyl-PLWKQQH-amide (HP7) were prepared similarly by capping the corresponding portion of HP35 with N-terminal acetyl and C-terminal amino groups, protonating H7, and embedding the peptide in a 15 Å sphere of 530 water molecules. The radius of the sphere was increased to 15.214 Å to model the lower density of water at 380 K. Following energy minimization at 30 K, ground-state simulations of HP7 were run for 8 ns at 280 K or for 6 ns at 380 K followed by 1 ns at 680 K, and then for an additional 4 ns at 380 K. The trajectories at 380 K also were continued to 8 ns without the excursion to 680 K.

All-atom MD simulations were propagated in 1 fs steps with ENZYQ and INDIP.[44] Briefly, the atomic charges and excitation energies of a subsystem consisting of W23, H27 or N27, and the contiguous amide and Cα atoms bordering each of these residues were treated quantum mechanically, while the MD force field was purely classical. Atomic coordinates and electric fields were saved at intervals of 100 ps during ENZYQ trajectories in the ground electronic state and used as starting points for trajectories of 500 ps in the tryptophan's lowest excited single state. Coordinates and fields were saved again at intervals of 0.5 ps during the excited-state trajectories and were passed to INDIP, which optimized the induced electric dipoles separately for the ground state, the first two excited $\pi-\pi^*$ states, and charge-transfer (CT) states in which an electron moved from the indole to the imidazolium ring or any of the amide groups in the quantum subsystem.

Electron-transfer rate constants were calculated with the expression

$$k_{et} = \frac{2\pi}{\hbar}\left\langle |V(t)|^2 \frac{\hbar\xi/2\pi}{|V(t)|^2 + \hbar\xi/2\pi}\rho_{FC}[\Delta E(t)]\right\rangle \quad (1)$$

where $\Delta E(t)$ is the time-dependent difference between the energies of the reactant and product electronic states, with induced dipoles optimized separately for each state, $V(t)$ is the electronic interaction matrix element (coupling factor) for the reaction, $\rho_{FC}[\Delta E(t)]$ is the Franck–Condon-weighted density of product vibronic states that are approximately degenerate with the reactant, ξ is a parameter related to the rate at which the vibronic states relax by dissipating energy to the surroundings, and the broken brackets denote an average over multiple MD trajectories in the reactant state.[44] Equation 1 interpolates smoothly between the Golden rule and adiabatic limits. By averaging over the conformational space of the reactant state, we avoid the need to assume that the potential energy surfaces of the reactant and product states have a simple quadratic dependence on a reaction coordinate. The weighted density of product states was written as follows:[44]

$$\rho_{FC}(\Delta E) = (2/\pi\sigma^2)^{1/2}\exp[-(\Delta E/\sigma)^2/2] /[1 + \exp(\Delta E/\delta)] \quad (2)$$

This expression recognizes that, when $\Delta E < 0$, transitions can occur to a manifold of excited vibrational levels of the product, with an increasing density of the manifold compensating partly for the decrease in the Franck–Condon factors as the reaction becomes progressively more exothermic. The values for ξ, σ, and δ (2.5×10^{13} cm^{-1} s^{-1}, 1.5×10^4 cm^{-1}, and 100 cm^{-1}, respectively) were taken from ref 44 with no special adjustments to fit the measured fluorescence yields for HP35 or HP7.

Fluorescence yields were calculated as

$$\Phi_f = k_f/(k_f + k_{nr} + k_{et}^{sum}) \quad (3)$$

where k_{et}^{sum} is the sum of the rate constants for the transfer of an electron from the excited indole ring of the tryptophan to the histidine imidazolium and the amide groups in the quantum system ($k_f = 6.11 \times 10^7$ s^{-1}, and $k_{nr} = 1.858 \times 10^8$ s^{-1}). The values for k_f and k_{nr}, taken again from ref 44, were assumed to be independent of temperature. The calculations therefore do not consider the transfer of an electron to the solvent, which

dx.doi.org/10.1021/bi5004712 | *Biochemistry* 2014, 53, 4503–4509

probably is negligible at 280 K but undergoes an increase in rate with an increase in temperature.[1,45] They also neglect excited states of the protein backbone and charge transfer between hydrogen-bonded amide groups of the backbone.[47] States of the latter type were found occasionally among the first dozen excited states but (in structures that had relaxed in the tryptophan's first $\pi-\pi^*$ state) were almost always considerably higher in energy than the lowest CT and $\pi-\pi^*$ states of the tryptophan. The calculations for the H27N peptide included the transfer of an electron from W23 to the side-chain amide of N27 as well as transfer to backbone amides.

Calculated rate constants, fluorescence yields, and other properties were averaged over the 1000 structures saved from each trajectory of HP35 in the excited state and then averaged for the excited-state trajectories embarking at corresponding points from five independent trajectories in the ground state at 280 K. The corresponding quantities for HP7 were averaged similarly over excited-state trajectories starting from 10 ground-state trajectories under each of the conditions considered (280 or 380 K, with or without 1 ns at 680 K). The symbols and error bars in the figures represent the mean and standard error of the mean (SEM) of the values for a given excitation point [SEM = $s/(n-1)^{1/2}$, where s is the sample standard deviation and n is the number of ground-state trajectories].

The ENZYQ/INDIP treatment was found to work well for calculating fluorescence yields in a set of 30 designed miniproteins.[44] Those proteins all resemble HP35 in having a tryptophan residue whose side chain is partly exposed to the solvent. They include systems in which the transfer of an electron to an imidazolium ring appears to account for most of the fluorescence quenching and others with a broad range of rate constants for the transfer of an electron to backbone amides or other groups. However, the ENZYMIX force field used in ENZYQ has been used mostly for calculations of electrostatic energies in proteins at moderate temperatures.[48,49] Although it reproduces the diffusion coefficient, electric dipole, and other properties of water well at 300 K,[44] it has not been tested extensively at higher temperatures.

Semiclassical electrostatic energies were calculated as

$$\Delta E_{\mathrm{elec}} = \sum_i (Q_i^{\mathrm{CT}} - Q_i^{\pi\pi^*}) \sum_j q_j/r_{ij} \qquad (4)$$

where Q_i^{CT} is the charge of quantum atom i when the system is in a given CT state and $Q_i^{\pi\pi^*}$ is the same for the lowest excited singlet $\pi-\pi^*$ state, each with induced dipoles optimized for that state; index i runs over the π atoms of the electron donor or acceptor group; q_j is the charge of nonquantum atom j of the protein or water; and r_{ij} is the distance between atoms i and j. Note that the second sum in eq 4 does not consider screening by the fields from induced dipoles. ΔE_{elec} was used only to obtain a qualitative picture of factors that affect the energy gap for electron transfer, not to calculate the actual ΔE for eq 1.

Figures 1 and 2 were drawn with VMD,[50] which uses STRIDE[51] to identify α-helices.

RESULTS AND DISCUSSION

Figure 3 shows the calculated quantum yield (Φ_f) of fluorescence from HP35 as a function of time in the ground state at 280 K, along with calculations for peptide fragment HP7 at 280 and 380 K with and without a 1 ns period at 680 K. The histidine side chain was protonated in all cases. Each value of Φ_f represents an average of calculations at 0.5 ps intervals

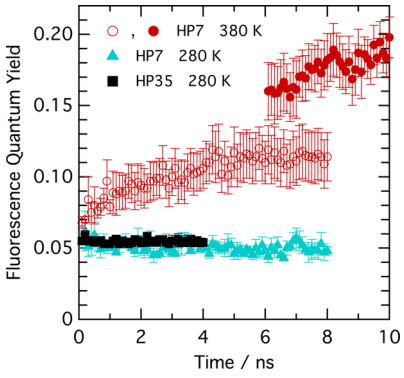

Figure 3. Calculated fluorescence yields as a function of time for HP35 at 280 K (black squares), HP7 at 280 K (cyan triangles), and HP7 at 380 K with and without a 1 ns excursion to 680 K at 6 ns (filled and empty red circles, respectively). The fluorescence yield calculated by eqs 1−3 was averaged over 500 ps trajectories in the lowest excited singlet state of the quantum system, following excitation from the ground state at each of the times indicated on the abscissa, and averaged over five independent trajectories for each of the systems at 280 K and 10 trajectories for the systems at 380 K. Fluorescence yields were not calculated during the period at 680 K.

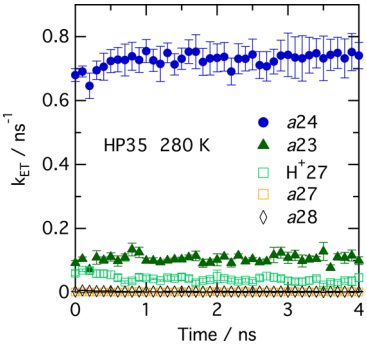

Figure 4. Calculated rate constants (k_{ET}) for electron transfer in HP35 at 280 K. The rate constants for transfer from the excited indole ring of W23 to the imidazolium side chain of H27 and the backbone amide groups of these residues (*a*23, *a*24, *a*27, and *a*28) are shown as light green empty squares, dark green filled triangles, blue filled circles, gold empty squares, and black empty diamonds, respectively. Each rate constant was averaged over multiple trajectories as in Figure 3.

during 500 ps trajectories in the tryptophan's lowest excited singlet state, beginning with excitation from the ground state at the time indicated on the abscissa. The total time available for unfolding at 380 K thus was, on average, 250 ps longer than the period in the ground state. This is comparable to the situation in a temperature-jump experiment, where the time in the excited state depends on the fluorescence lifetime and the length of the excitation flash or shutter used to measure the fluorescence. The time indicated on the abscissa also does not include the period at 680 K in some of the trajectories. Inspection of Figure 3 shows that the calculated values of Φ_f for HP35 and HP7 remain essentially constant during the trajectories at 280 K (filled black squares and cyan triangles). The calculated fluorescence yield for HP35 at 280 K (0.055 ± 0.001) agrees well with the measured yield (0.052),[1] and the Φ_f for HP7 at this temperature is essentially the same. At 380 K, however, Φ_f for HP7 increases with time (empty red circles), and including a 1 ns period at 680 K causes an additional increase in the yield calculated after the temperature is returned to 380 K (filled red circles). The quantum yield for HP7 during

dx.doi.org/10.1021/bi5004712 | *Biochemistry* 2014, 53, 4503−4509

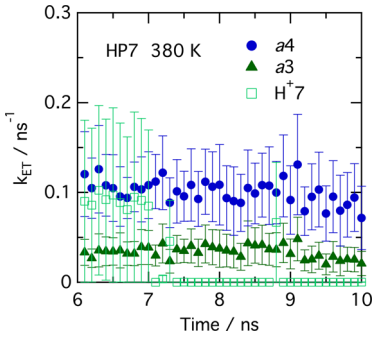

Figure 5. Calculated rate constants (k_{ET}) for electron transfer in HP7 at 380 K. The rate constants for transfer from the excited indole ring of W3 to the imidazolium side chain of H7 and the backbone amide groups *a*3 and *a*4 are shown as light green empty squares, dark green filled triangles, and blue filled circles, respectively. The time period represented is the 4 ns period at 380 K following 6 ns at 380 K and 1 ns at 680 K (see the filled red circles in Figure 3). Each rate constant was averaged over multiple trajectories as in Figure 3. Note that the vertical scale is expanded 3-fold compared to that in Figure 4. The rate constants for transfer to *a*7 and *a*8 (not shown) also were included in the calculations of fluorescence yields but were almost always $<10^{-4}$ ns^{-1}.

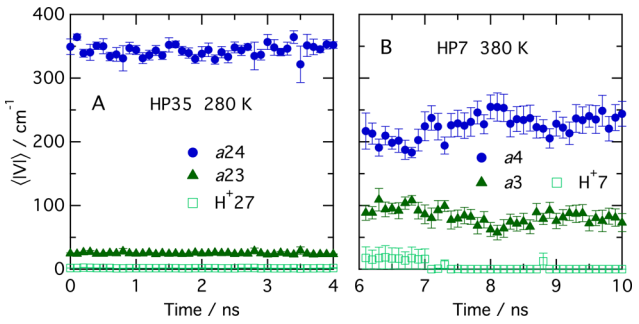

Figure 6. Mean interaction matrix elements ($|V_{ET}|$) for the transfer of an electron from the indole of W23 to amide *a*23 (dark green triangles), amide *a*24 (blue circles), and the imidazolium ring of H27 (light green squares) in HP35 (A) and from the indole of W3 to amide *a*3 (dark green triangles), amide *a*4 (blue circles), and the imidazolium ring of H7 (light green squares) in HP7 (B). $|V_{ET}|$ was evaluated in the excited state and averaged over multiple trajectories as in Figure 3. The time period shown in panel B is the same as that in Figure 5.

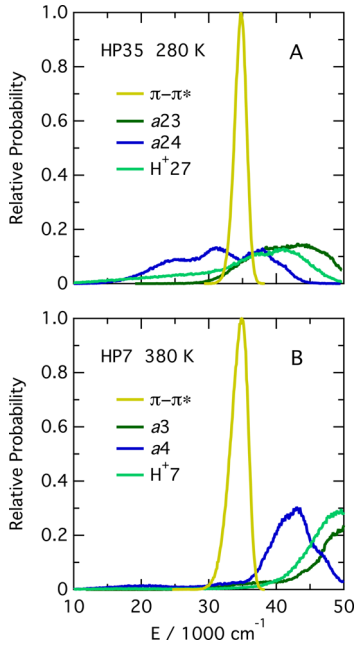

Figure 7. (A) Distribution functions of the energy (E) of the first excited singlet state (π–π^*, yellow-green) and the CT states in which an electron moves from the W23 indole of HP35 to amide *a*23 (dark green), amide *a*24 (blue), or the H27 imidazolium ring (light green). The distribution functions include all the trajectories of HP35 in the excited state at 280 K. (B) Distribution functions of E for the first excited singlet state (π–π^*, yellow-green) and the CT states in which an electron moves from the W3 indole of H7 to amide *a*3 (dark green), amide *a*4 (blue), or the H7 imidazolium ring (light green). These distributions include all the excited-state trajectories beginning during the last 2 ns of the trajectories that were propagated in the ground state for 6 ns at 380 K, 1 ns at 680 K, and 4 ns at 380 K. Energies are expressed relative to the energy of the ground state.

the last 2 ns of the latter trajectories is comparable to the value reported for *N*-acetyltryptophanylamide at room temperature (0.18).[1,45]

The calculations of Φ_f shown in Figure 3 consider quenching of fluorescence by the transfer of an electron from the excited indole ring of the tryptophan to either the imidazolium side chain of the histidine or the backbone amide groups of these residues. Figure 4 shows the calculated rate constants (k_{ET}) for the individual reactions in HP35 at 280 K. The dominant process clearly is transfer to the amide on the carboxyl side of W23 (*a*24), with transfer to the amide on the amino side (*a*23) coming in second. The transfer of an electron to the imidazolium group (H27) evidently makes only a minor contribution. Transfer to either of the amides of H27 is insignificant, having an average rate constant of 0.0013 ns^{-1} for *a*27 and 0.0027 ns^{-1} for *a*28. In unfolded peptide HP7, k_{ET} for transfer to amide *a*4 is $\sim^1/_8$ of that for the corresponding amide *a*28 in HP35, and k_{ET} for transfer to *a*3 is $\sim^1/_2$ of that for *a*27 (Figure 5). The rate constant for transfer to the imidazolium group (H7) fluctuates during the first nanosecond after HP7 is cooled from 680 to 380 K (between 6 and 7 ns in Figure 5) but then decreases as well.

Several factors contribute to the high rate of transfer of an electron to amide *a*24 in the folded protein. First, the electron donor and acceptor are closer together than they are for the other reactions. The mean distance between the centers of mass of the indole ring and *a*24 during the ground-state trajectories of HP35 at 280 K was 4.30 Å, compared to 5.62 Å for *a*23 and 9.10 Å for the imidazolium ring (SEM < 0.01 Å in all cases). The short distance results in a large matrix element (coupling factor, V) for electron transfer (Figure 6A). The mean coupling factor for the transfer of an electron to *a*4 decreases by $\sim^1/_3$ in unfolded HP7 (Figure 6B). However, this is unlikely to account for the decrease in the rate of electron transfer, because the calculated rate is almost independent of the coupling factor as long as $|V|$ remains above ~30 cm^{-1}.[44] Note also that the k_{ET} for the transfer of an electron to *a*3 in HP7 is smaller than that for transfer to *a*23 in HP35, even though $|V|$ for this reaction is ~3 times larger in HP7 (Figure 6B).

Enhanced coupling factors for the transfer of an electron to the imidazolium group were seen in some of the trajectories during the first nanosecond after HP7 was cooled from 680 to 380 K (Figure 6B). These reflect transient conformations that bring the imidazolium and indole rings closer together and probably account for the higher rate of transfer of charge to the histidine during this period (see Figure 5).

dx.doi.org/10.1021/bi5004712 | *Biochemistry* 2014, 53, 4503–4509

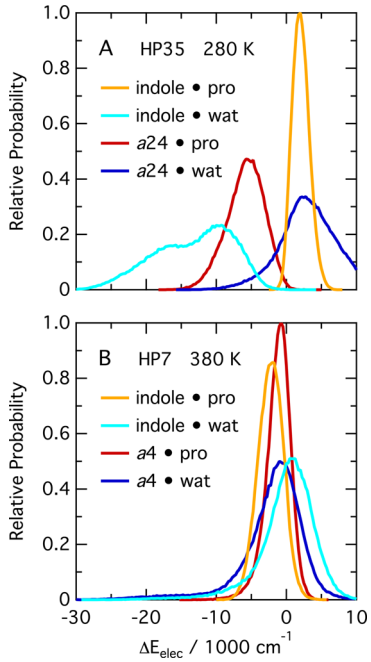

Figure 8. (A) Changes in electrostatic interactions of the W23 indole ring with the nonquantum protein atoms (orange) and water (cyan) and in interactions of amide *a*24 with the nonquantum protein atoms (red) and water (blue) for the transfer of an electron from the indole to *a*24 in HP35 at 280 K. The distribution functions include all the trajectories of HP35 in the excited state at 280 K. (B) Changes in electrostatic interactions of the W3 indole ring with the nonquantum protein atoms (orange) and water (cyan) and in interactions of amide *a*4 with the nonquantum protein atoms (red) and water (blue) for the transfer of an electron from the indole to *a*4 in HP7 at 380 K. These distribution functions include all the excited-state trajectories beginning during the last 2 ns of the trajectories that were propagated in the ground state for 6 ns at 380 K, 1 ns at 680 K, and 4 ns at 380 K. The difference between the electrostatic energies of the product (CT) and reactant (excited) states (ΔE_{elec}) was calculated by eq 4 from the quantum charges of the indole or amide and the classical charges of the water and other protein atoms.

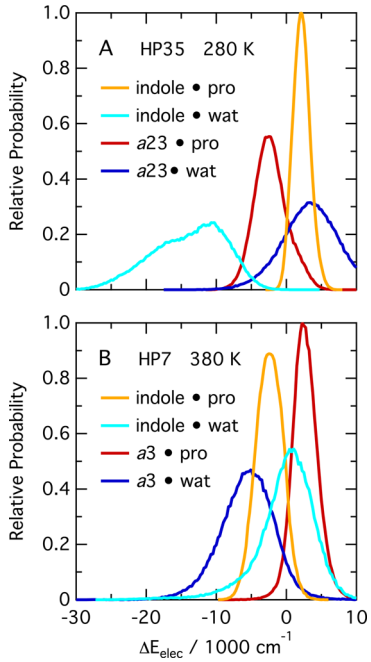

Figure 9. Same as Figure 8, but for the transfer of an electron from the W23 indole to *a*23 in HP35 (A) and from the W3 indole to *a*3 in HP7 (B). Although the indole ring interacts with the same sets of atoms as in Figure 8, and ΔE_{elec} does not include interactions with induced dipoles of the nonquantum atoms in either case, the atomic charges of the indole are modified slightly by the different induced dipoles.

More importantly, the transfer of an electron from the excited indole to *a*24 tends to be strongly favorable energetically, whereas transfer to the imidazolium group or the other amides tends to be unfavorable (Figure 7A). The energy gaps for all the reactions shift upward in unfolded HP7, so that the transfer of an electron to amide *a*4 also becomes endothermic (Figure 7B).

The favorable energetics of the transfer of an electron from the indole to amide *a*24 in HP35 can be attributed partly to electrostatic interactions of the indole ring with water and partly to interactions of *a*24 with other atoms of the protein (Figure 8A). The corresponding interactions become much weaker in unfolded HP7 (Figure 8B). Interactions of the amide with water shift in the opposite direction, as do interactions of the indole with other atoms of the protein, but these are relatively weak in both cases. Qualitatively similar changes in electrostatic interactions occur for the transfer of an electron to amide *a*23 (Figure 9). The changes in the electrostatic interactions of other protein atoms with *a*23 and *a*24 probably result largely from the loss of the net dipole from helix α3, which is oriented in a way that favors the reduction of the amides in HP35 (see Figure 1). The changing interactions of the indole ring with water are more complex and, judging from the shapes of the distribution functions in Figures 8 and 9, include the development of surroundings that are more homogeneous overall, even though the side chain experiences a broader spectrum of torsional angles.

Fluorescence yields calculated for HP35 with H27 unprotonated and for the peptide containing asparagine in place of H27 are provided in Figure S1 of the Supporting Information. Comparison with Figure 3 shows that changing the protonation state of H27 had little effect on the calculated yields, in qualitative accord with experiment.[46] However, the calculations did not reproduce the higher fluorescence of the peptide with asparagine at position 27, possibly because the computer model used was generated from the crystal structure of HP35 with histidine at this position and could require longer simulations to capture all of the structural differences between the two peptides.

■ CONCLUSIONS

Although fluorescence quenching probably does not involve the transfer of an electron from the indole ring to H27 as had been expected, tryptophan fluorescence nevertheless appears to provide a good probe of the conformation of HP35 in the region of helix α3. Altered electrostatic interactions decrease the level of quenching of fluorescence by making the transfer of an electron to amides *a*23 and *a*24 energetically less favorable in the unfolded protein.

■ ASSOCIATED CONTENT

Supporting Information

Figure S1. This material is available free of charge via the Internet at http://pubs.acs.org.

dx.doi.org/10.1021/bi5004712 | *Biochemistry* 2014, 53, 4503−4509

AUTHOR INFORMATION

Corresponding Author

*E-mail: parson@u.washington.edu. Phone: (206) 523-0142.

Funding

Supported by National Science Foundation Grant 0641640.

Notes

The author declares no competing financial interest.

ACKNOWLEDGMENTS

I thank Jose Tusell and Andy McMillan for helpful discussions and Jan Kubelka for providing unpublished data on the effects of pH and the H27N mutation.

ABBREVIATIONS

CT, charge transfer; HP35, 35-residue C-terminal portion of villin with a protonated histidine in place of asparagine 27; HP7, *N*-acetyl-PLWKQQH-amide with histidine 7 protonated; MD, molecular dynamics; SEM, standard error of the mean; Φ_f, quantum yield of fluorescence.

REFERENCES

(1) Kubelka, J., Eaton, W. A., and Hofrichter, J. (2003) Experimental tests of villin subdomain folding simulations. *J. Mol. Biol. 329*, 625−630.

(2) McKnight, C. J., Doering, D. S., Matsudaira, P. T., and Kim, P. S. (1996) A thermostable 35-residue subdomain within villin headpiece. *J. Mol. Biol. 260*, 126−134.

(3) McKnight, C. J., Matsudaira, P. T., and Kim, P. S. (1997) NMR structure of the 35-residue villin headpiece subdomain. *Nat. Struct. Biol. 4*, 180−184.

(4) Bi, Y., Cho, J. H., Kim, E. Y., Shan, B., Schindlelin, H., et al. (2007) Rational design, structural and thermodynamic characterization of a hyperstable variant of the villin headpiece helical subdomain. *Biochemistry 46*, 7497−7505.

(5) Cellmer, T., Buscaglia, M., Henry, E. R., Hofrichter, J., and Eaton, W. A. (2011) Making connections between ultrafast protein folding kinetics and molecular dynamics simulations. *Proc. Natl. Acad. Sci. U.S.A. 108*, 6103−6108.

(6) Frank, B. S., Vardar, D., Buckley, D. A., and McKnight, C. J. (2002) The role of aromatic residues in the hydrophobic core of the villin headpiece subdomain. *Protein Sci. 11*, 680−687.

(7) Kubelka, J., Chiu, T. K., Davies, D. R., Eaton, W. A., and Hofrichter, J. (2006) Sub-microsecond protein folding. *J. Mol. Biol. 359*, 546−553.

(8) Kubelka, J., Henry, E. R., Cellmer, T., Hofrichter, J., and Eaton, W. A. (2008) Chemical, physical, and theoretical kinetics of an ultrafast folding protein. *Proc. Natl. Acad. Sci. U.S.A. 105*, 18655−18662.

(9) Chung, J. K., Thielges, M. C., Lynch, S. R., and Fayer, M. D. (2012) Fast dynamics of HP35 for folded and urea-unfolded conditions. *J. Phys. Chem. B 116*, 11024−11031.

(10) Serrano, A. L., Bilsel, O., and Gai, F. (2012) Native state conformational heterogeneity of HP35 revealed by time-resolved FRET. *J. Phys. Chem. B 116*, 10631−10638.

(11) Reiner, A., Henklein, P., and Kiefhaber, T. (2010) An unlocking/relocking barrier in conformational fluctuations of villin headpiece subdomain. *Proc. Natl. Acad. Sci. U.S.A. 107*, 4955−4960.

(12) Glasscock, J. M., Zhu, Y., Chowdhury, P., Tang, J., and Gai, F. (2008) Using an amino acid fluorescence resonance energy transfer pair to probe protein unfolding: Application to the villin headpiece subdomain and the LysM domain. *Biochemistry 47*, 11070−11076.

(13) Zhu, L., Ghosh, K., King, M., Cellmer, T., Bakajin, O., et al. (2011) Evidence of multiple folding pathways for the villin headpiece subdomain. *J. Phys. Chem. B 115*, 12632−12637.

(14) Tang, Y., Rigotti, D. J., Fairman, R., and Raleigh, D. P. (2004) Peptide models provide evidence for significant structure in the denatured state of a rapidly folding protein: The villin headpiece subdomain. *Biochemistry 43*, 3264−3272.

(15) Brewer, S. H., Vu, D. M., Tang, Y., Li, Y., Franzen, S., et al. (2005) Effect of modulating unfolded state structure on the folding kinetics of the villin headpiece subdomain. *Proc. Natl. Acad. Sci. U.S.A. 102*, 16662−16667.

(16) Buscaglia, M., Kubelka, J., Eaton, W. A., and Hofrichter, J. (2005) Determination of ultrafast protein folding rates from loop formation dynamics. *J. Mol. Biol. 347*, 657−664.

(17) Chiu, T. K., Kubelka, J., Herbst-Irmer, R., Eaton, W. A., Hofrichter, J., et al. (2005) High-resolution X-ray crystal structures of the villin headpiece subdomain, an ultrafast folding protein. *Proc. Natl. Acad. Sci. U.S.A. 102*, 7517−7522.

(18) Godoy-Ruiz, R., Henry, E. R., Kubelka, J., Hofrichter, J., Muñoz, V., et al. (2008) Estimating free-energy barrier heights for an ultrafast folding protein from calorimetric and kinetic data. *J. Phys. Chem. B 112*, 5938−5949.

(19) Bunagan, M. R., Gao, J., Kelly, J. W., and Gai, F. (2009) Probing the folding transition state structure of the villin headpiece subdomain via side chain and backbone mutagenesis. *J. Am. Chem. Soc. 131*, 7470−7426.

(20) Cellmer, T., Henry, E. R., Kubelka, J., Hofrichter, J., and Eaton, W. A. (2007) Relaxation rate for an ultrafast folding protein is independent of chemical denaturant concentration. *J. Am. Chem. Soc. 129*, 14565−14565.

(21) Duan, Y., and Kollman, P. A. (1998) Pathways to a protein folding intermediate observed in a 1-microsecond simulation in aqueous solution. *Science 282*, 740−744.

(22) Zagrovic, B., Snow, C. D., Shirts, M. R., and Pande, V. S. (2002) Simulation of folding of a small α-helical protein in atomistic detail using worldwide-distributed computing. *J. Mol. Biol. 323*, 927−937.

(23) Jayachandran, G., Vishal, V., and Pande, V. S. (2006) Using massively parallel simulation and Markovian models to study protein folding: Examining the dynamics of the villin headpiece. *J. Chem. Phys. 124*, 164902.

(24) Jayachandran, G., Vishal, V., Garcia, A. E., and Pande, V. S. (2007) Local structure formation in simulations of two small proteins. *J. Struct. Biol. 157*, 491−499.

(25) Ensign, D. L., Kasson, P. M., and Pande, V. S. (2007) Heterogeneity even at the speed limit of folding: Large-scale molecular dynamics study of a fast-folding variant of the villin headpiece. *J. Mol. Biol. 374*, 806−816.

(26) Lei, H., and Duan, Y. (2007) Two-stage folding of HP-35 from ab initio simulations. *J. Mol. Biol. 370*, 196−206.

(27) Lei, H., Wu, C., Liu, H., and Duan, Y. (2007) Folding free-energy landscape of villin headpiece subdomain from molecular dynamics simulations. *Proc. Natl. Acad. Sci. U.S.A. 104*, 4925−4930.

(28) Yang, J. S., Wallin, S., and Shakhnovich, E. I. (2008) Universality and diversity of folding mechanisms for three-helix bundle proteins. *Proc. Natl. Acad. Sci. U.S.A. 105*, 895−900.

(29) Tusell, J. R., and Callis, P. R. (2012) Simulations of tryptophan fluorescence dynamics during folding of the villin headpiece. *J. Phys. Chem. B 116*, 2586−2594.

(30) Freddolino, P. L., and Schulten, K. (2009) Common structural transitions in explicit-solvent simulations of villin headpiece folding. *Biophys. J. 97*, 2338−2347.

(31) Lee, I. H., Kim, S. Y., and Lee, J. (2010) Dynamic folding pathway models of the villin headpiece subdomain (HP-36) structre. *J. Comput. Chem. 31*, 57−65.

(32) Jang, S., Kim, E., Shin, S., and Pak, Y. (2003) Ab initio folding of helix bundle proteins using molecular dynamics simulations. *J. Am. Chem. Soc. 125*, 14841−14846.

(33) Lei, H., Su, Y., Jin, L., and Duan, Y. (2010) Folding network of villin headpiece subdomain. *Biophys. J. 99*, 3374−3384.

(34) Sullivan, D. C., and Kuntz, I. D. (2001) Conformational spaces of proteins. *Proteins 42*, 495−511.

(35) Herges, T., and Wenzel, W. (2005) Free-energy landscape of the villin headpiece in an all-atom force field. *Structure 13*, 661−668.

(36) Piana, S., Lindorff-Larsen, K., and Shaw, D. E. (2012) Protein folding kinetics and thermodynamics from atomistic simulation. *Proc. Natl. Acad. Sci. U.S.A. 109*, 17845−17850.
(37) Duan, Y., Wang, L., and Kollman, P. A. (1998) The early stage of folding of villin headpiece subdomain observed in a 200-ns fully solvated molecular dynamics simulation. *Proc. Natl. Acad. Sci. U.S.A. 95*, 9897−9902.
(38) Shen, M. Y., and Freed, K. F. (2002) All-atom fast protein folding simulations: The villin headpiece. *Proteins 49*, 439−445.
(39) Fernández, A., Shen, M. Y., Colubri, A., Sosnick, T. R., Berry, R. S., et al. (2003) Large-scale context in protein folding: Villin headpiece. *Biochemistry 42*, 664−671.
(40) Steiner, R., and Kirby, E. P. (1969) Interaction of the ground and excited states of indole derivatives with electron scavengers. *J. Phys. Chem. 73*, 4130−4135.
(41) Yu, H.-T., Colucci, W. J., McLaughlin, M. L., and Barkley, M. D. (1992) Fluorescence quenching in indoles by excited-state proton transfer. *J. Am. Chem. Soc. 114*, 8449−8454.
(42) De Beuckeleer, K., Volckaert, G., and Engelborghs, Y. (1999) Time resolved fluorescence and phosphorescence properties of the individual tryptophan residues of barnase: Evidence for protein-protein interactions. *Proteins 36*, 42−53.
(43) Loewenthal, R., Sancho, J., and Fersht, A. R. (1991) Fluorescence spectrum of barnase: Contributions of three tryptophan residues and a histidine-related pH dependence. *Biochemistry 30*, 6775−6779.
(44) McMillan, A. W., Kier, B. L., Shu, I., Byrne, A., Andersen, N. H., et al. (2013) Fluorescence of tryptophan in designed hairpin and Trp-cage miniproteins: Measurements of fluorescence yields and calculations by quantum mechanical molecular dynamics simulations. *J. Phys. Chem. B 117*, 1790−1809.
(45) Thompson, P. A., Muñoz, V., Jas, G. S., Henry, E. R., Eaton, W. A., et al. (2000) The helix-coil kinetics of a heteropeptide. *J. Phys. Chem. B 104*, 378−389.
(46) Personal communication in 2014 with J. Kubelka, University of Wyoming, Laramie, WY.
(47) Shemesh, D., Sobolewski, A. L., and Domcke, W. (2010) Role of excited-state hydrogen detachment and hydrogen-transfer processes for the excited-state deactivation of an aromatic dipeptide: N-acetyl tryptophan methyl amide. *Phys. Chem. Chem. Phys. 12*, 4899−4905.
(48) Lee, F. S., Chu, Z. T., and Warshel, A. (1993) Microscopic and semimicroscopic calculations of electrostatic energies in proteins by the POLARIS and ENZYMIX programs. *J. Comput. Chem. 14*, 161−185.
(49) Warshel, A., Sharma, P. K., Kato, M., and Parson, W. W. (2006) Modeling electrostatic effects in proteins. *Biochim. Biophys. Acta 1746*, 1647−1676.
(50) Humphrey, W., Dalke, A., and Schulten, K. (1996) VMD: Visual molecular dynamics. *J. Mol. Graphics 14*, 33−38.
(51) Frishman, D., and Argos, P. (1995) Knowledge-based secondary structure assignment. *Proteins: Struct., Funct., Genet. 23*, 566−579.